ISSN (Print) : 0974-6846
Indian Journal of Science and Technology, *Vol 10(26), DOI: 10.17485/ijst/2017/v10i26/98766, July 2017* ISSN (Online) : 0974-5645

Production of $KMnO_4$ Modified Activated Carbon Fiber Filter from Pineapple Leaf Carbon Fiber for Fe^{3+} and Ca^{2+} Ions Adsorption

Sumrit Mopoung* **and Pornsawan Amornsakchai**

Department of Chemistry, Naresuan University, Phitsanulok, Thailand; sumritm@nu.ac.th, pornsawana@nu.ac.th

Abstract

Objectives: The effects of ratios of $KMnO_4$ modified activated carbon fiber, zeolite, and sintering temperature for filter preparation were studies. The Fe^{3+} and Ca^{2+} ions removal by filter were also evaluated. **Methods/Statistical analysis:** The filters were characterized by XRD, FTIR, SEM-EDS, and BET analyzer. The percent drying shrinkage, percent firing shrinkage, percent total shrinkage, percent mass yield, density, and hardness were measured. The adsorption isotherms for Fe^{3+} and Ca^{2+} ions of the modified filter materials were also studied. **Findings:** The shrinkages and density properties increased with increasing sintering temperature and decreasing carbon fiber content, but hardness and mass yields showed a reverse trend. The filter has high content of MnO_2, Si and Al oxides, P- and O-contain functional groups, montmorillonite, and kaolinite. The BET, pore volume and pore size of the sintered filter materials are quite lower than those of the starting materials due to the effects of the functional groups on the filter surface. **Application/Improvements:** Langmuir isotherm and Freundlich isotherm were fitted for both Fe^{3+} and Ca^{2+} adsorption by the modified filter with theoretical maximum adsorption capacity of 45.25 and 23.53 mg/g, respectively.

Keywords: Activated Carbon Fiber Filter, Adsorption Isotherm, Ca^{2+}, Fe^{3+}, $KMnO_4$, Pineapple Leaf Carbon Fiber

1. Introduction

Various technologies for drinking water production are available with low cost and operating without electricity[1]. Activated carbon is usually used for water purification. It is made from materials with high carbon content through carbonization and an activation process. A porous structure and its adsorption properties can be obtained in carbonaceous materials either via chemical or physical activation[2]. Adsorption using activated carbon is strongly influenced by the surface area and surface charge[3]. Activated carbon fiber filters have also been used in a wide range of applications including air purification, dehumidification, and water purification, due to their large specific surface area, high adsorption capacity and rate, and specific surface reactivity[4]. Natural bio-fiber, as a starting material for activated carbon, can be produced from agricultural waste. Bio-fiber with low cost and high abundance can be extracted from pineapple leaf as reported[5,6]. Pineapple leaf fiber exhibits high specific strength and stiffness. It has a ribbon-like structure and consist of a vascular bundle system present in the form of bunches of fibrous cells, which are obtained after mechanical removal of all of the epidermal tissues[7]. It has many potential applications similar to other natural fibers such as plastic reinforcement, sound and thermal insulations[8]. For water filter production, activated carbon or activated carbon fiber can be mixed with clay minerals to from the final composite. Clay minerals are the most important inorganic components in soil due to their excellent mechanical and chemical properties[9]. Kaolinite ($A1_2O_3{\cdot}2SiO_2{\cdot}2H_2O$) is the principal mineral in clay. It is a widely available, low cost, and high abundance material[10]. It consists of silica tetrahedron layers linked to alumina octahedron layers through hydrogen bonding between the tetrahedrons' basal oxygen and the hydroxyls from the octahedron layers[3]. The other clay mineral that has been widely used as filter is zeolite. Zeolites have a great capacity for cationic exchange and an affinity for heavy metals with high surface area and unique

* *Author for correspondence*

pore characteristics. They also have three-dimensional structures consisting of silica and alumina tetrahedrons with a great number of pores in the structure[3]. The general formula for a zeolite is $M_{2/n}O{\cdot}Al_2O_3{\cdot}xSiO_2{\cdot}yH_2O$ where M is any alkali or alkaline earth element, n is the valence charge on that element, x varies from 2 to 10 and y varies from 2 to 7. The Al_2O_3 and SiO_2 are structural cations because they form the tetrahedral framework with oxygen[11]. Zeolites have a negative charge (generated by isomorphous substitution of Si^{4+} by Al^{3+}), which is counter balanced by native cations (Na^+, K^+, Ca^{2+} and Mg^{2+}) and water molecules in their pores and channels. Zeolites have been used for coal steam gas water treatment[12], for removal of heavy metals (As, Cd, Cr, Cs, Cu, Fe, Hg, Mn, Ni, Pb, Sr, W and Zn) and ionic species (ammonium, chloride, fluoride, nitrate, phosphate and sulphate) from industrial sludge's, acid mine drainage, and for treatment of wastewater from domestic and industrial sources. In addition, fly ash zeolites find their application as sorbent medium in permeable reactive barriers and contaminant barrier liners for immobilizing the contaminant plume in soil[11]. Bentonite also has good sorbent properties for cationic pollutants such as high cation exchange capacity, reduction/elimination of bleeding, enhanced mechanical strength, optimal pore size and consequently higher adsorption efficiency, better stability and durability, reusability, larger surface area, and even comparatively lower cost for water treatment. Bentonite is one of the most widely used, abundant, and low-cost natural clay mineral[13].

For drinking water treatment, oxidation agents such as chlorine, ozone, or permanganate have been used to oxidize macro molecular organic materials and to convert them into biodegradable low molecular weight compounds, which can be combined with coagulation/flocculation process[14]. $KMnO_4$ is widely used in drinking water treatment to strengthen and improve the removal of contaminants. It is supposed to react with organic matter in water, and some $KMnO_4$ should be reduced to products, such as MnO_2 or other hydrated oxides[15]. Manganese oxide (MnO_2), which has low cost and is environmentally friendly, has been used for doping with transition metals on internal surfaces of macroporous carbon for super capacitors and oxygen reduction reaction electro catalysts[16].

The natural water, groundwater, and wastewater from industries and communities have a high content of Fe and Ca. Fe is found in groundwater in its most soluble form, Fe^{2+} ions, and in the oxide form, Fe_2O_3[17]. Iron is also present in high concentration in waste effluents from steel tempering, coal coking, and mining industries. Iron can have a detrimental influence on the taste of water. Fe^{3+} ions in human blood are toxic to tissues and organs[18]. In severe iron poisoning, much of the damage to the gastrointestinal tract and liver may be the result of highly localized iron concentration and free radical production leading to heptatoxicity through lipid peroxidation and the destruction of the hepatic mitochondria. As a result of the iron storage disease caused due to iron poisoning develops and the liver becomes cirrhotic. Hepatomia, the primary cancer of the liver, has become the most common cause of death among patients with hemochromatosis. This is an iron storage disease that results from the inability of the intestine to keep out unnecessary iron. Instead, iron gets accumulated in the liver causing siderosis[19]. Iron in drinking water and water supplies causes many problems, such as reddish color, bad odor, metallic turbidity, and staining of laundry. Iron removal is among the most problematic issues for making of potable water. Its main issues involve taste, visual effects, and clogging. The presence of dissolved iron influences the taste and aesthetic quality of water. Depending on the type and amount of iron, people may notice a metallic taste and red discoloration. Furthermore, residual iron at levels above 0.3 mg/dm^3 may stain surfaces and clothes[1].

There are several methods for removal of iron from drinking water like ion exchange and water softening, activated carbon and other filtration materials, supercritical fluid extraction, bioremediation and limestone treatment, oxidation by aeration, chlorination, ozonation followed by filtration, by ash, by aerated granular filter, by adsorption, and by manganese greensand (through oxidation and filtration)[1]. Soluble iron is also oxidized and precipitated by contact with higher oxides of manganese on the greensand granules. Precipitates are then filtered and removed by backwashing[1]. Water softener removes Fe, which is in the dissolved form. Softening also removes calcium and magnesium ions, which are the primary minerals responsible for hard water. The treatment process consists of passing the water through an ion exchange resin bed. The Fe ions as well as calcium and magnesium ions in the water are exchanged for sodium (Na^+) ions, which have been temporarily stored in the resin material. As the hardness and Fe are removed from

the water, sodium is added proportionally[1]. The most effective processes for the removal of these contaminants seem to be the use of activated carbons as highly porous materials as they have an extremely high surface area for contaminant adsorption[1]. Ceramic-packed biotrickling filter, which contains an immobilized activated sludge, has also been set up for water purification[20]. The double imprinted sorbent with chelating diamines[21], nano-hydroxyapatite chitin/chitosan hybrid biocomposites[19] were also used for Fe^{3+} ion adsorption.

In this work, activated carbon fiber filter from pineapple leaf fiber carbon doped with $KMnO_4$ was prepared. Activated carbon fiber filter was formed by mixing the plant material with clay, zeolite, bentonite, and borax (as fluxing agent). The effects of $KMnO_4$ and sintering temperature were studies. The filter products were characterized by XRD, FTIR, SEM-EDS, and BET analyzer. The Fe^{3+} and Ca^{2+} ion removal by the filter was studied as well.

2. Materials and Methods

2.1 Activated Carbon Fiber Preparation

Pineapple leaf fiber was collected after a mechanical milling process. Fresh pineapple leaves, which contain approximately 85% water, were cut to a length of 5 mm and milled with a disc mill. The milled materials were cleaned with water and air dried at room temperature for 3 days. The resulting dried crumb was ground with a high-speed grinder consisting of a stainless steel bowl and a rotating blade. The ground leaf is composed of fibrous and non-fibrous materials. After that, pineapple leaf fiber was oven (SL 1375 SHEL LAB 1350 FX, USA) dried at 105 °C for 6 hours. Sieving the material with steel wire sieve (mesh number 60) separated the fibrous and non-fibrous materials. The dried pineapple fibrous material contains approximately 71% of cellulose, 20% of hemicelluloses, and 2% of lignin by weight[5].

The dried pineapple leaf fiber was then carbonized at 500°C in an electric furnace (Fisher Scientific Isotemp® Muffle Furnace). The temperature was initially increased at a rate of 10°C/min and then kept constant for 1 h. The pineapple leaf carbon fiber was impregnated with 85% phosphoric acid using a weight/volume ratio of 1:1. The impregnated mixtures were oven dried at 105°C for 1 day and then activated at 500°C under partial oxygen of atmosphere. The temperature was also increased with a rate of 10°C/min up to 500°C and kept constant for 1 h. After that, the activated carbon fiber was modified with 5%wt of $KMnO_4$ and oven dried at 105°C for 1 day.

2.2 Filter Preparation

Zeolite (commercial grade), bentonite (commercial grade), and local clay (obtained from Tambol Tapoh, Muang District, Phitsanulok Province, Thailand), were ground and sieved (Laboratory test sieve, Retsch, Germany) to 200 mesh. These materials were mixed together with $KMnO_4$ modified activated pineapple leaf fiber carbon (40, 50, or 60wt %) to prepare mixtures containing zeolite (10, 20, or 30wt %), bentonite (10wt %), clay (10wt %), and borax ($Na_2B_4O_7 \cdot 10H_2O$) as the fluxing agent (10%wt) Table 1. The mixtures of all starting materials were wetted with

Figure 1. Samples of the rod form of the filters before sintering (a) and after sintering at 500°C (b), 600°C (c), and (d) 700°C.

Table 1. The ratios of raw starting materials in filter mixtures

No. samples	Ratios of raw materials in mixtures of filter (%wt)				
	$KMnO_4$ modified activated carbon fiber	Zeolite	Bentonite	Local clay	Borax
1	60	10	10	10	10
2	50	20	10	10	10
3	40	30	10	10	10

water (20% by volume) and then pressed into a PVC pipe (φ = 12.7 mm, long = 50 mm) as shown in Figure 1(a). The wetted samples were dried in an oven for 24 h. The dried samples were then placed into a ceramic box and covered with foil, quartz powder, and closed by a lid. These samples were then sintered in an electric furnace under a reducing atmosphere at temperatures of 500°C, 600°C, or 700°C with 1 h soaking time. The percent of drying shrinkage and percent of firing shrinkage of the samples were measured by the methods of de in[22,23] respectively. The percent mass yields of the sintered filters were also measured. The sintered samples were characterized by X-ray powder diffractometer (XRD, PW 3040/60, X' Pert Pro MPD) with a Cu tube anode, a Fourier transform infrared spectrometer (Spectrum GX, Perkin Elmer), scanning electron microscope equipped with energy dispersive spectrometer (SEM-EDS, LEO 1455 VP), and BET analyzer (Micromeritics TriStar II).

2.3 Fe Adsorption Experiments

The 1000 mg/dm³ Fe^{3+} stock solution was prepared from 0.4827 g of iron(III) chloride hexahydrate (Merck, Germany) dissolved in deionized water, acidified with 1 cm³ of 1 M HCl added, and diluted to 100 cm³ with deionized water. Further solutions (3, 5, 7 and 10 mg/dm³) were prepared from the stock solution by successive dilution.

Batch Fe^{3+} adsorption experiments were performed using the method of[24]. The filters (0.1 g) were added to 50 cm³ of Fe^{3+} solutions (3, 5, 7, 10 mg/dm³) in a conical flasks and shaken continuously at 120 rpm at a temperature of 32 ± 2 °C. Following the adsorption, the aqueous phases were separated by centrifugation at 4000 rpm for 10 min and the final concentrations of Fe^{3+} ion in the solutions were determined by FAAS (Varian SpectrAA 220, Australia) with air–acetylene and cathode on Fe-hollow cathode lamp at 248.3 nm.

The amounts of adsorbed Fe^{3+} ions were calculated by the difference in initial and final concentrations. The effects of pH (2-9) and contact time (20–180 min) were studied to achieve optimum performance of Fe^{3+} adsorption.

2.4 Calcium Adsorption Experiments

Batch calcium adsorption experiments were performed following the method of[25]. Water with Ca^{2+} ion concentrations of 9.7, 19.4, 24.2, 36.1, and 48.0 mg/dm³ were prepared by using $CaCl_2$ (Merck, Germany) dissolved in distilled water. The pH of the synthetic and tap waters was between 8.0 and 8.7. For Ca^{2+} adsorption experiments, filter (0.1 g) was added to 50 cm³ of Ca^{2+} solution (9.7, 19.4, 24.2, 36.1, and 48.0 mg/dm³) in a conical flask. The suspension was shaken continuously at 120 rpm and a temperature of 32±2 °C. Following the adsorption, the aqueous phase was separated by centrifugation at 4000 rpm for 10 min and the final concentration of Ca^{2+} ion in the solution was determined by FAAS with air–acetylene and cathode on a Ca-hollow cathode lamp at 427.7 nm. The adsorbed amount of Ca^{2+} was calculated as well that of Fe^{3+}.

2.5 Removal Efficiency of Fe^{3+} and Ca^{2+} Ions

Final concentrations (C_f) of Fe^{3+} or Ca^{2+} were measured for the calculation of Fe^{3+} and Ca^{2+} removal percentages as shown in the eq. (1)[26]:

$$\text{Removal}\% = ((C_o - C_f)/C_o) \times 100 \quad (1)$$

where C_o is the initial Fe^{3+} or Ca^{2+} ion concentration (mg/dm³); C_f is the final Fe^{3+} or Ca^{2+} ion concentration (mg/dm³). The adsorption capacity (Q_t, mg/g) at any time was calculated using a mass balance equation as shown in the eq. (2)[26]:

$$Q_t = (C_o - C_f) \times (V/W) \quad (2)$$

Where V is the volume of the solution (dm³); W is the mass of dry modified pineapple carbon fiber filter used (g).

2.6 Adsorption Isotherms

All of the experimental adsorption data were fitted with both the Langmuir equation and the Freundlich equation.

The rearranged Langmuir equation is:

$$Q_e = (Q_{max} K_L C_e)/(1 + K_L C_e) \quad (3)$$

where Q_e (mg/g) is the amount of solution adsorbed per unit mass of adsorbent, C_e (mg/dm^3) is the Fe^{3+} or Ca^{2+} equilibrium concentration, Q_{max} (mg/g) is the maximum Fe^{3+} or Ca^{2+} amount that forms a complete monolayer on the surface, and K_L (dm^3/mg) is the Langmuir constant related to adsorption heat. The linear form of this equation after rearrangement is:

$$C_e/Q_e = 1/(Q_{max} K_L) + C_e/Q_{max} \quad (4)$$

The constants Q_{max} and K_L can be determined from the slope and intercept of plotting C_e/Q_e against C_e[27], respectively.

Freundlich model is used to estimate the adsorption intensity of $KMnO_4$ modified pineapple leaf carbon fiber filter towards the Fe^{3+} or Ca^{2+} ions and the equations is as follows:

$$Q_e = K_F C_o^{(1/n)} \quad (5)$$

This equation is conveniently used in linear form as[27]:

$$\log Q_e = \log K_F + 1/n \log C_e \quad (6)$$

where Q_e and C_e have the same definitions as those in the Langmuir equation cited above. K_F and n are Freundlich constants related to adsorption capacity and heterogeneity factor, respectively. The constants K_F and n can be determined from the intercept and slope of plotting log C_e against log Q_e, respectively.

3. Results and Discussion

3.1 The Physical Properties and Mass Yield

From Figure 1, it can be seen that the surfaces of the sintered filters have a brick color (Figure 1(b), Figure 1(c), and Figure 1(d)) as compared to the starting filters, which have a black color (Figure 1(a)). It shows that the some carbon fibers of the filters have undergone thermal degradation. It is also apparent that more degradation is observed as the sintering temperature is increased from 500°C to 700°C. However, the inside texture of the sintered filters is still partially black. This shows that the carbon fibers are most degraded on the filter surface, which could be explained by clay mineral layers acting as insulators and a mass transport barrier to the volatile products generated during thermal decomposition[28]. The brick color of the sintered filter is due to the presence of iron oxide[28] during sintering, which originates from the Fe content of the starting clay minerals. The black color intensities of the sintered filters decrease with increasing sintering temperature from 500 °C to 700 °C (Figure 1(b), Figure 1(c), Figure 1(d)). It was observed that the filter sintered at 700 °C is quite broken, which means that the filter fabricated with sintering at 700 °C possesses low hardness. As can be seen in Table 2, the drying shrinkages of the filters are increasing as the content of the fiber carbon is decreased and the zeolite content increased. Likewise, the firing shrinkage, increases with decreasing carbon fiber content and increasing sintering temperature. As a result, the total shrinkages are increased with increasing sintering temperature and decreasing carbon fiber content of the starting filters. On the other hand, the mass yields of the filters after sintering are decreased with increasing sintering temperature and increasing carbon fiber content of starting filters. The mass loss is related to the loss of surface-absorbed water (free water), interlayer water, dehydroxylation of the clay sheets[29], and carbon[28]. The densities of the sintered filters increase with increasing sintering temperature and decreasing carbon fiber content. This trend is correlated with the increase of total of shrinkage. This result is due to the release of volatile matter from all starting materials at high sintering temperatures[30]. Another reason is the presence of the clay minerals, which are thermally stable inorganic materials with high density[31]. The hardness of the sintered filters also decreased with increasing sintering temperature and increasing carbon fiber content. This is attributed to the amount of carbon fiber of sintered filter, which decreases with increasing sintering temperature and decreasing carbon fiber content of starting filter mixtures. The remaining carbon fiber in the sintered filters ensures interfacial interaction between carbon fiber and clay matrix by interlocking[32] within the sintered filter. However at the sintering temperature of 700 °C, the hardness of sintered filter is lower than the limit set by the Thai Industrial Standards Institute (7.1380 kg/cm^2)[33].

Table 2. Percent of drying shrinkage, firing shrinkage, total shrinkage, and mass yield of mixture samples of filters with sintering at 500-700°C

No. Samples	Temperature °C	% drying shrinkage	% firing shrinkage	% total of shrinkage	Mass yield (wt%)	Density (g/cm^3)	Hardness kg/cm^2
1	500	2.91	3.21	6.12	76.27	0.27	14.25
1	600	2.87	3.92	6.79	62.80	0.35	10.27
1	700	2.95	4.03	6.98	58.34	0.41	7.04
2	500	3.25	4.01	7.26	79.67	0.32	13.85
2	600	3.32	4.72	8.04	67.53	0.46	11.02
2	700	3.21	5.34	8.55	63.92	0.52	7.01
3	500	4.00	4.17	8.17	80.35	0.42	12.54
3	600	4.12	4.84	8.96	72.95	0.56	9.43
3	700	4.03	5.52	9.55	68.75	0.68	6.97

3.2 Elemental Composition

Table 3 shows the EDS analysis results for selected samples. It shows that the carbon content of carbonized pineapple leaf fiber after carbonization at 500°C is increased in comparison to the starting pineapple leaf fiber. This is because the volatile matter from the pineapple leaf fiber undergoes thermal degradation[30]. The carbon content decreased after activation with H_3PO_4, and modification with $KMnO_4$, and further more decreased with mixing in of clay minerals. This is attributed to the thermal degradation and oxidation of carbon content[28] leading to a higher content of clay minerals. After the H_3PO_4 activation, the P content of the pineapple leaf carbon fiber is significantly increased. This indicates that the P is accumulated on the carbon fiber. Furthermore, after $KMnO_4$ modification, contents of K and Mn elements of the modified activated carbon fiber are also increased. This shows that K and Mn are also accumulated on the carbon fiber. It was seen that the P element remained on the carbon fiber after $KMnO_4$ modification. It can be concluded that the P atom formed a chemical bond to the carbon fiber, which is manifested by the presence of functional groups on the surface such as P=O, P—O—C linkage, P=OOH, and P—O—P[34]. In the case of the sintered filters, it was found that the content of Si and Al elements has increased as these elements originate from the clay minerals. This resulted in a further reduction of the C content. However, the K, Mn, and P elements remain in the filter. Analysis of the surface of the carbon fibers of the filter with EDS confirmed that the K, Mn, and P atoms are still present on the carbon fiber of the filter after sintering. Many of the samples contain a high amount of oxygen. This finding points to the presence oxygen containing functional surface groups such as carboxyl, carbonyl, phenol, lactone, and other[35], being present in all of the samples. These results are linked to the physical properties and mass yield (Table 2).

3.3 FTIR Analysis

Figure 2 shows the FTIR transmissions for activated carbon fiber after H_3PO_4 activation, $KMnO_4$ modified pineapple carbon fiber, and $KMnO_4$ modified activated carbon fiber filter. It compares the pineapple leaf carbon fiber after H_3PO_4 activation using a 1:1 (volume: weight) ratio of 85% H_3PO_4 and pineapple leaf carbon fiber, the 5wt% $KMnO_4$ modified activated carbon fiber, and the 5wt% $KMnO_4$ modified fiber carbon filter after mixing with clay, zeolite, and bentonite. For activated carbon fiber (Figure 2(a)), the spectrum shows the peaks of OH vibrations (broad band between 2550-3600 cm^{-1}), P–H vibrations (at 2350 cm^{-1}), C=O group vibrations (at 1625 cm^{-1}), PO_4^{3-} vibrations (at 1160, 1000, 875, and 490 cm^{-1})[36], and C–O group vibrations (which overlap with phosphate bands at 1160 cm^{-1})[19]. After $KMnO_4$ modification (Figure 2(b)), the modified pineapple carbon fiber also shows peaks of O–H stretching (at 3400–2500 cm^{-1}), O–H bending (at 1225 cm^{-1}), and C–O stretching (at 1100 cm^{-1})[37], which as appeared as a result of $KMnO_4$ activation. Vibrations belonging to the PO_4^{3-} group were also found at about 1000 cm^{-1}. The presence of MnO_2 in $KMnO_4$ modified activated carbon fibers was confirmed by peaks in range 400 to 800 cm^{-1} at wave numbers such as 650 cm^{-1}, 500 cm^{-1}, and 450 cm^{-1} [38–40]. In the case of the filters (Figure 2(c)), the IR spectrum shows the peaks of SiO–H groups (at 3750 cm^{-1}), tetrahedral Al ions (at about 1000 cm^{-1}), and Al–O or Si–O symmetric stretching

vibrations (at 800 and 460 cm^{-1})[41], which originate from clay, zeolite, and bentonite. Vibrations assigned to carboxylates and also B–O, originating from $Na_2B_4O_7$ (at weak peaks 1575 and 1385 cm^{-1})[42] were also found. The presence of CO or PO_4^{3-} groups was also confirmed in the filters (at about 1000 cm^{-1}), and C–O deformation vibration (at 617 cm^{-1})[15]. The results from FTIR analysis give further support to the content of various elements in the materials originally assigned from the EDS analysis (Table 3).

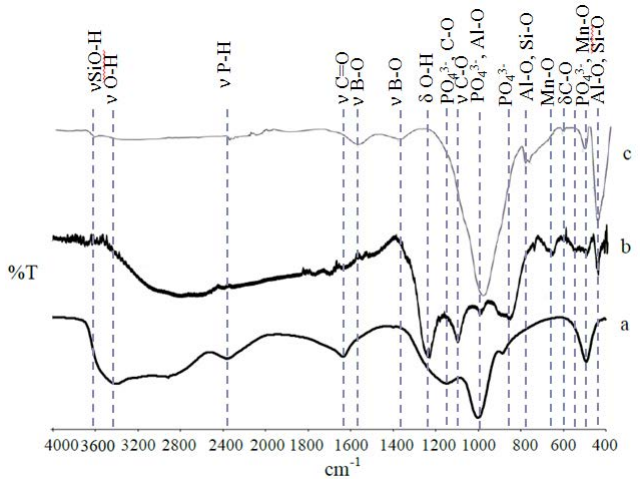

Figure 2. FTIR spectra of (a) activated carbon after H_3PO_4 activation, (b) $KMnO_4$ modified pineapple carbon fiber, (c) $KMnO_4$ modified activated carbon fiber filter.

3.4 X-Ray Diffraction Analysis

The XRD diffraction of activated carbon fibers after H_3PO_4 activation Figure 3(a) shows peaks of amorphous carbon (2θ = ~24° and 44°)[43], and the P–C (sharp weak peak at 25°)[33]. The diffraction peaks of amorphous carbon are also observed in $KMnO_4$ modified activated carbon fibers (Figure 3(b)) and filters (Figure 3(c)). This confirms that the activated carbon fiber is still exists in filters after sintering at 500°C. The $KMnO_4$ modified activated carbon fiber (Figure 3(b)) shows XRD diffraction of MnO_2 at 23°, 27°, 36.5°, 43°, and 65.5°[16,44]. The P–C peaks at 25° are still present in the $KMnO_4$ modified activated carbon fibers. This reveals that the P atom is still present in the $KMnO_4$ modified activated carbon fiber. For filters, the XRD diffraction (Figure 3(c)) shows peaks of quartz (22°, 27°, 30°, 35.5°, 40°, 50°, 53°, and 60°), montmorillonite (7.5°, 18°, 28°, 30°, and 43°)[45]. Kaolinite is also found in the filter at 26°, 28°, 39°, and 57°[46]. These components originate from raw clay minerals. Sodium metaborate ($NaBO_2$) was found as well (43° and 53°)[33] and it comes from borax fluxing agent. It was seen that some diffraction peaks corresponding to P and MnO_2 were not detected in the filters. This is because these spectra are dominated by the peaks of clay minerals as reported[44]. The peaks at 30°, 32°, 33.3°, and 48° are attributed to calcite[46].

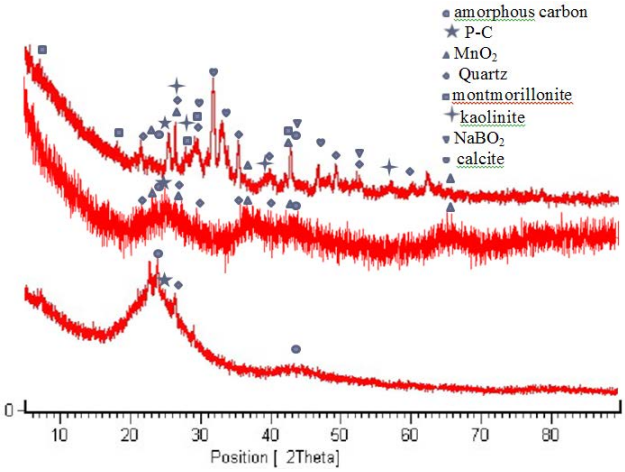

Figure 3. The XRD diffraction patterns of (a) activated carbon fiber after H_3PO_4 activation (b) $KMnO_4$ modified pineapple activated carbon fiber (c) $KMnO_4$ modified pineapple activated carbon fiber filter.

Table 3. Elemental composition of samples determined by EDS analysis

Samples	wt% of elements									
	C	O	Si	K	Mn	Mg	Al	P	Ca	Fe
PF	47.31	50.47	0.21	0.22	0.03	0.05	0.42	0.44	0.32	0.02
PCF at 500 °C	68.27	22.61	1.62	2.20	0.31	0.68	0.79	1.66	0.96	0.19
PACF (H_3PO_4) at 500	58.92	25.02	1.45	1.57	0.25	0.43	1.09	9.60	0.78	0.14
5KPACF	55.56	26.14	1.17	5.65	6.82	0.14	0.52	3.20	0.63	0.06
5KPACF Filter at 500 °C	24.14	22.90	20.37	2.78	3.36	0.63	19.26	1.28	1.87	0.63
Focus on surface of 5KPACF filter at 500 °C	54.57	28.57	1.35	3.46	5.16	1.01	0.71	2.41	2.61	0.54

PF= pineapple leaf fiber, PCF= pineapple leaf carbon fiber, PACF= pineapple leaf activated carbon fiber, 5KPACF= 5wt% $KMnO_4$ modified pineapple leaf activated carbon fiber

3.5 Textural Characteristics.

Table 4 shows BET surface area, pore volume, and average pore size of a select group of samples. It can be seen that activated carbon fiber, after H_3PO_4 activation at 500°C, has higher surface area and pore volume than carbon fiber carbonized at 500 °C. However, the trend of the average pore size is reverse. This is due to the presence of H_3PO_4 in the impregnated carbon fibers during such high temperature conditions, which cause structural expansion in the activated carbon fiber that is being activated. This results in the surface area and the pore volume being increased. New micropores are created below 500 °C, which is consistent with a report[47]. After modified of the activated carbon fibers with $KMnO_4$ the surface area and pore volume of the modified activated carbon fibers are lowered. On the other hand average pore size of the material is increased. It seems that $KMnO_4$ modification leads to the formation of bigger mesopores, which leads to a lower surface area and pore volume[48]. Finally, surface area and average pore size of the filters prepared using sintering at 500 °C are even lower. However, the pore volume of these materials is relatively higher. This is attributed to the coalescence behavior[49] between clay minerals and modified activated carbon fibers in the sintered filters, which results in lowering of surface area and average pore size of the filter. In contrast, the pore volume of sintered filters is increased. This is attributed to the degradation of volatile matter contained in clay minerals and carbon[28–29] of the starting filter. Another reason is the porosity of zeolite with high content of the glassy phase after sintering, which exhibits high porosity[50].

3.6 SEM-EDS Analysis

Figure 4 shows the SEM morphology of a final filter. It can

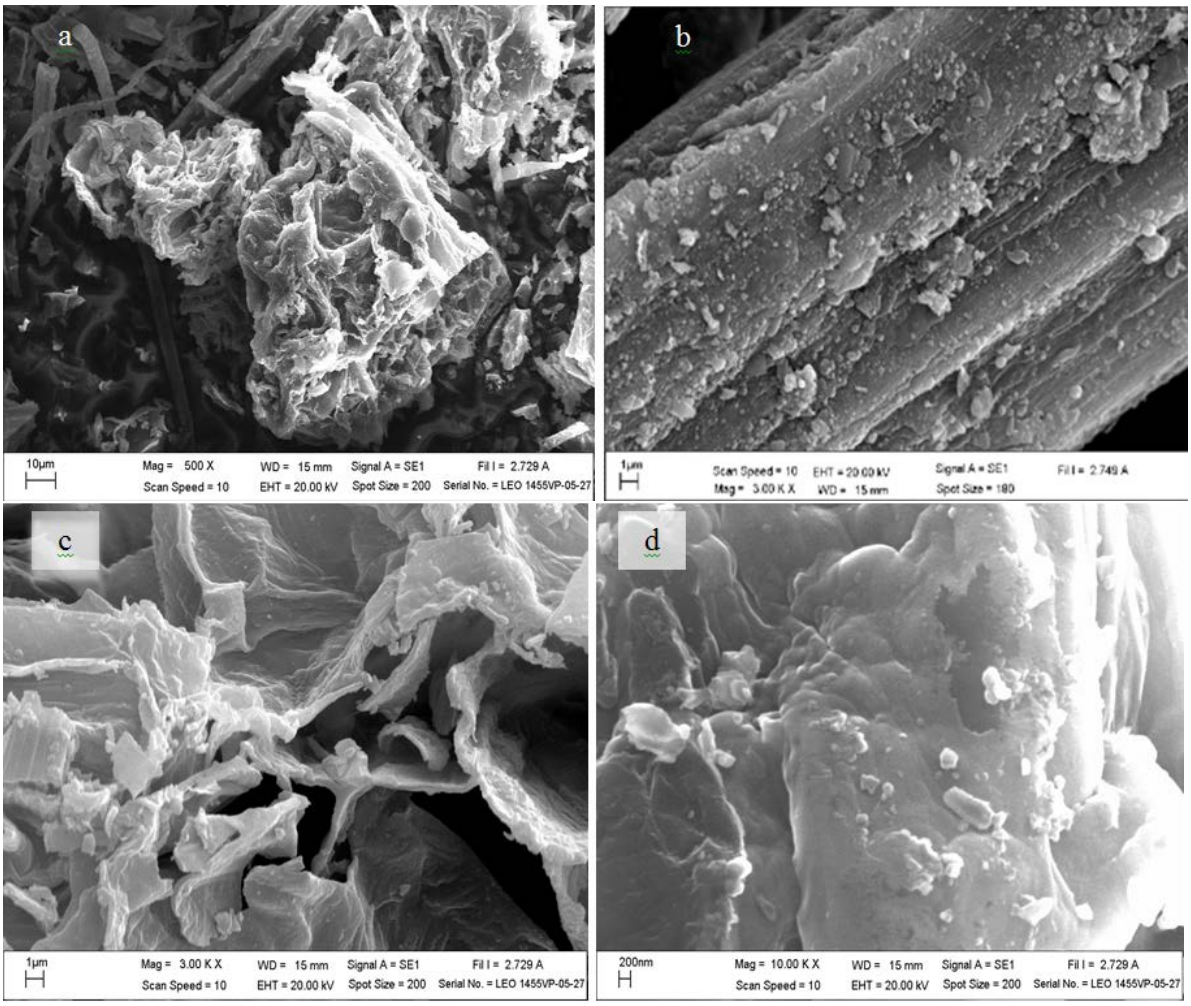

Figure 4. SEM morphology of filter after sintering at 500°C, (a) overview at 500x, (b) view of carbon fiber only (c) surface texture at 3000x and (d) surface texture at 10000x.

nly (c)

Table 4. BET surface area, pore volume, and average pore size of the samples

Samples	BET surface area (m^2/g)	pore volume (cm^3/g)	Average pore size (nm)
PCF at 500 °C	106.7863	0.067077	2.51258
PACF at 500 °C	534.3411	0.25933	1.9413
5KPACF	211.9945	0.050387	4.2014
5KPACF Filter at 500 °C sintering	167.4968	0.08698	2.0772

be seen that the carbon fibers are distributed throughout the filter texture (overview in Figure 4(a)). It was shown that the carbon fibers exist in the filter after sintering at 500°C. It can be seen that small particles with different sizes are present on the surface of $KMnO_4$ modified activated carbon fiber. Based on the EDS analysis of this surface, the elemental composition of the surface of this carbon fiber is C, O, Mg, Al, Si, P, K, Mn, Ca, and Fe (Table 3). These elements originate from all of the raw materials e.g. Carbon fibers, H_3PO_4, $KMnO_4$, clay, zeolite, and bentonite. As focus view on the clay minerals with 3000x expansion (Figure 4(c)) shows a porous structure with wallplate wave character. When an expansion of the wallplate structure is made at magnification of 10000x (Figure 4(d)) wave surface with small particle and micropores can be observed.

3.7 Effect of Contact Time and pH on Adsorption of Fe^{3+} Ions

Figure 5(a) shows the effect of contact time of 5 mg/dm^3 Fe^{3+} solution with filter at pH 5. It can be seen that the equilibrium for Fe^{3+} ion adsorption is achieved after about 60 min contact time with about 95% efficiency of removal. Figure 5(b) confirms that the maximum pH for Fe^{3+} ion adsorption by these filters is about 5, which is due to low hydrogen ion competition from the solution. At pH >5, the Fe^{3+} adsorption becomes rapidly less efficient, which is due to the increased Fe^{3+} hydrolysis[51]. On the other hand, the Fe^{3+} adsorption at pH < 5 is also low. This could be explained by protonation of active sites of the filter at low, resulting in competition between H^+ ions and Fe^{3+} ions for the binding sites[21]. Therefore pH 5.0 was selected for the further Fe^{3+} adsorption experiments.

3.8 Fe^{3+} Ions Adsorption Isotherm

Figure 6 shows Langmuir adsorption isotherm plot (Figure 6(a)) and Freundlich adsorption isotherm plot (Figure 6(b)) of Fe^{3+} adsorption for 5% $KMnO_4$ modified activated carbon fiber filter. It shows that the data of Fe^{3+} adsorption by the filter can be fitted with both the Langmuir isotherm and the Freundlich isotherm (R^2 = 0.9999 and 0.9978, respectively). The Q_{max} and K_L values are 45.25 mg/g and 221.00 dm^3/g, respectively. The theoretical maximum adsorption capacity for Fe^{3+} on $KMnO_4$ modified activated carbon filter is higher than that of nano-hydroxyapatite chitin/chitosan hybrid biocomposites (4.238-6.753 mg/g)[19], carboxymethylated chitosan hydrogels (18.5 mg/g)[18], and double template imprinted sorbent (36.90 ± 3.16 mg/g)[21]. It is also higher than for $KMnO_4$ modified carbon prepared

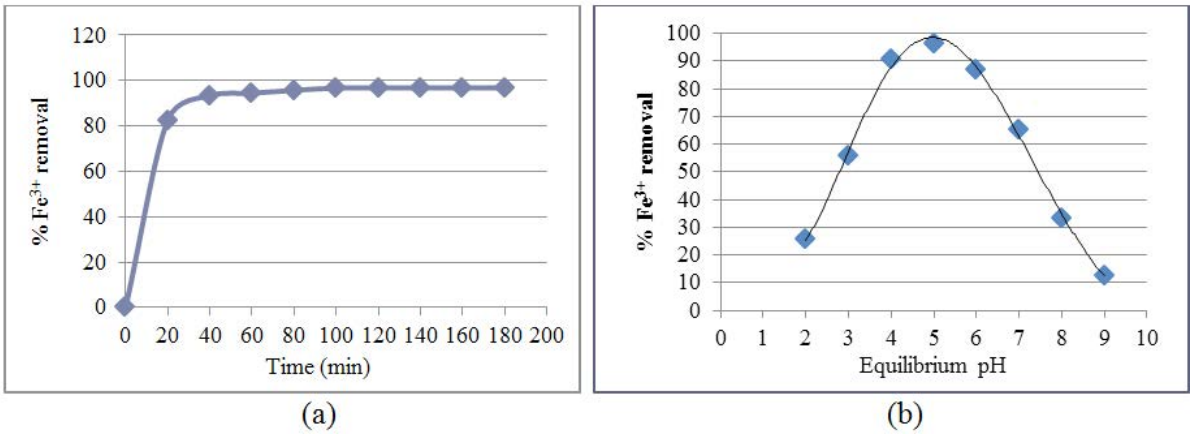

Figure 5. Effect of (a) contact time and (b) pH, on Fe^{3+} removal efficiency.

from waste of pineapple leaf fiber without clay minerals (25.25 mg/g)[52]. It was shown that the mineral clays have a significant effect on Fe^{3+} adsorption due to high density of functional groups and porous structure as showed in Figure 2 and Table 3. The dimensionless parameter (R_L) values of Fe^{3+} Langmuir adsorption isotherm (0.0004523-0.00151) of the filters indicate the adsorption to be favourable ($0 < R_L < 1$)[51] under these conditions. This means that the Langmuir adsorption isotherm describes well the Fe^{3+} adsorption process by $KMnO_4$ modified activated pineapple carbon fiber filter, using the assumption that the Fe^{3+} ions are homogeneously distributed in a monolayer[53] over the $KMnO_4$ modified filter surface. In case of the Freundlich isotherm, the fitting of the data provided K_F and n with values of 44.6684 $dm^3{}^{(1/n)}$ $mg^{(1-1/n)}/g$ and 28.409, respectively. The high values of these two parameters reveal that the adsorption capacity and adsorption intensity of Fe^{3+} ions on the modified filter are high and a very strong adsorption is observed[53]. It is noteworthy that the value of n is significantly greater than 1, which indicates very high heterogeneity[27] of the filter. It was seen that both adsorption isotherm models fit well the Fe^{3+} adsorption data of the filter. This is due to the fact that a low Fe^{3+} concentration (5 mg/dm^3) was used for this adsorption experiment. Thus, Fe^{3+} ions may adsorb in a monolayer on filter, which has heterogeneous surface as shown in SEM image (Figure 4).

3.9 Adsorption of Ca^{2+} Ions

Figure 7 shows the Ca^{2+} adsorption isotherm plots. It can be seen that they are similar to the Fe^{3+} adsorption plots. Both the Langmuir isotherm and the Freundlich isotherm models could be fitted with Ca^{2+} adsorption data. But R^2 values for both these isotherms are lower than for the Fe^{3+} adsorption isotherms. This is because the Ca^{2+} concentration used in the experiments (9.7-48.0 mg/dm^3) is quite higher than the Fe^{3+} concentration (3-9 mg/dm^3) used for adsorption experiments. It was observed that the R^2 value for the Freundlich isotherm of the Ca^{2+} adsorption data is relatively higher than that of the Langmuir isotherm. It may be attributed to the Ca^{2+} adsorption on the filter taking place in a more complicated structure than just a monolayer. The other reason is attributed to the Ca^{2+} adsorption experiment, which follows the method of[25]. In this experimental method, the total hardness of the solutions is maintained at a constant level using Ca^{2+}, Mg^{2+}, and $NaHCO_3$. Therefore the Ca^{2+}adsorption experiments took place under competition from Mg^{2+} ions, which are assumed to have a higher adsorption rate than Ca^{2+} [54] As a result, the five parameters obtained from the two isotherms for Ca^{2+} adsorption quite lower than for the Fe^{3+} adsorption isotherms. The values of Q_{max}, K_L, R_L, K_F, and n are = 23.53 mg/g, 1.6410 dm^3/g, 0.01254-0.0591, 12.5199 $dm^3{}^{(1/n)}$ $mg^{(1-1/n)}/g$, and 2.7465, respectively. This reveals that Ca^{2+} adsorption, according to the Langmuir isotherm, is still favourable under these conditions. However, adsorption capacity, adsorption intensity, and adsorption force for Ca^{2+} ions on the modified filter is lower than for Fe^{3+} adsorption. It may also be due to the competition between Ca^{2+} and Mg^{2+} ions. The Ca^{2+}

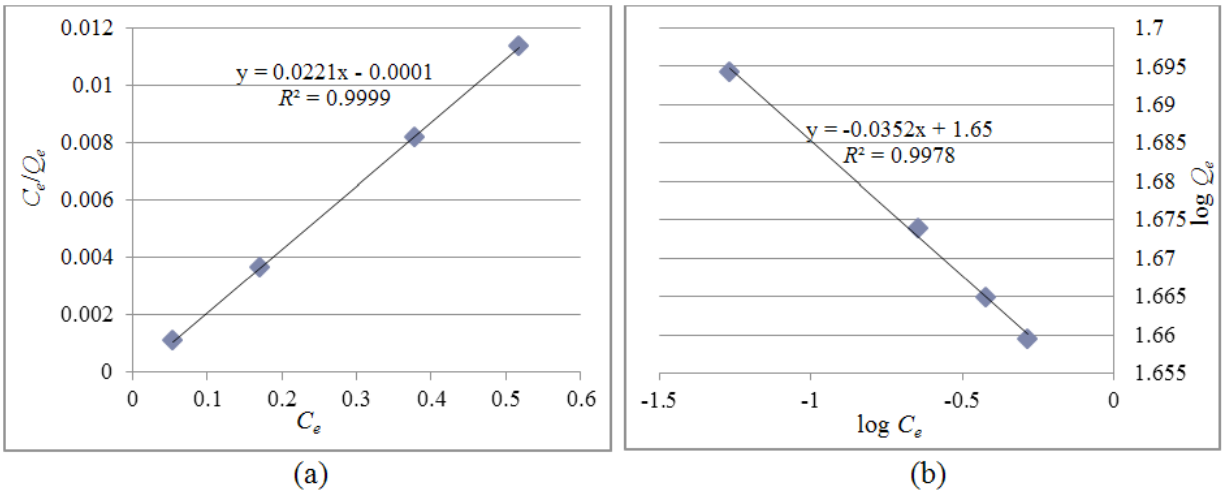

Figure 6. Fe^{3+} Langmuir adsorption isotherm plot (a) and Fe^{3+} Freundlich adsorption isotherm plot (b) for 5% $KMnO_4$ modified activated carbon fiber filter.

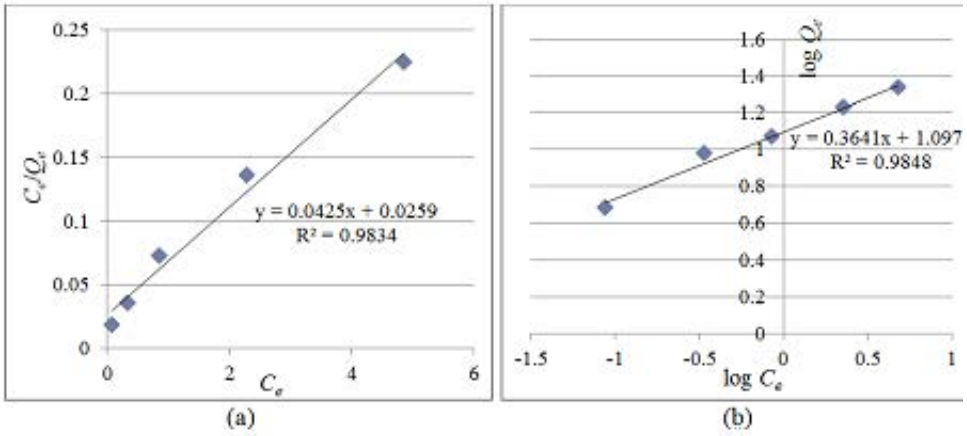

Figure 7. Langmuir isotherm plots (a), and Freundlich isotherm plot (b) for Ca^{2+} ion adsorption by 5% $KMnO_4$ modified pineapple activated carbon fiber filter.

adsorption on $KMnO_4$ modified activated carbon filter is also higher than on $KMnO_4$ modified carbon prepared from waste of pineapple leaf fiber without clay minerals (4.37-8.95 mg/g)[55].

4. Conclusion

Shrinkages (6.12-9.55%) and densities (0.27-0.68 g/cm^3) of modified filters increased with increasing sintering temperature (500 °C to 700 °C) and decreasing carbon fiber content (60 wt% to 40 wt%). On the other hand, hardness (form 14.25 kg/cm^2 to 6.97 kg/cm^2) and mass yields (from 80.00% to 58.34%) of modified filter exhibited a reverse trend. The values of these properties are within the requirements of the Thai Industrial Standards Institute, except for those prepared with sintering at 700 °C. The interfacial interactions between carbon fibers and clay matrix were improved by interlocking in the interior of the sintered filter. Many functional surface groups, oxide compounds, and clay minerals exist in filters such as MnO_2, Si and Al oxides, P- and O-containing functional groups, montmorillonite, and kaolinite. These constituents have a positive effect on the adsorption properties for Fe^{3+} and Ca^{2+} by enabling ion exchange or complexation. The values of BET (167.50 m^3/g), pore volume (0.08698 cm^3/g) and average pore size (2.0772 nm) of sintered filters are quite lower than those of the starting materials due to occlusion of surface functional groups and composites on filter surface. Langmuir isotherm and Freundlich isotherm were fitted for both Fe^{3+} and Ca^{2+} adsorption with high R^2 values. However, the parameter values from both Langmuir isotherm and Freundlich isotherm of Ca^{2+} adsorption are significantly lower than for Fe^{3+} adsorption. The theoretical maximum adsorption capacities of Fe^{3+} and Ca^{2+} for the modified filter are 45.25 and 23.53 mg/g, respectively, which are higher than for $KMnO_4$ modified carbon prepared from waste of pineapple leaf fiber without clay minerals. This emphasizes that the clay minerals have an effect on metal ion adsorption.

5. Acknowledgement

This work was financially supported by the National Research Council of Thailand and Naresuan University. The authors acknowledge Science lab center, Faculty of Science, Naresuan University for all of the analysis.

6. References

1. Chaturvedi S, Dave PN. Removal of iron for safe drinking water. Desalination, Elsevier, ScienceDirect. 2012 Oct 1; 303:1–11. Crossref.
2. Shamsuddin MS, Yusoff NRN, Sulaiman MA. Synthesis and characterization of activated carbon produced from kenaf core fiber using H_3PO_4 activation. Procedia Chemistry, Elsevier, ScienceDirect. 2016; 19:558–65. Crossref.
3. Magriotis ZM, Leal PVB, Sales DPF, Papini RM, Viana PRM, Arroyo PA. A comparative study for the removal of mining wastewater by kaolinite, activated carbon and beta zeolite. Applied Clay Science, Elsevier, ScienceDirect. 2014; 91–92:55–62. Crossref.
4. Sim KM, Kim KH, Hwang GB, Seo SC, Bae GN, Jung JH. Development and evaluation of antimicrobial activated

carbon fiber filters using Sophora flavescens nanoparticles. Science of the Total Environment, Elsevier, ScienceDirect. 2014 Sep 15; 493:291–7. Crossref.
5. Kengkhetkit N, Amornsakchai T. A new approach to ''Greening" plastic composites using pineapple leaf waste for performance and cost effectiveness. Materials and Design, Elsevier, ScienceDirect. 2014 Mar; 55:292–9. Crossref.
6. Yusof Y, Yahya SA, Adam A. Novel technology for sustainable pineapple leaf fibers productions. Procedia CIRP, Elsevier, ScienceDirect. 2015; 26:756–60. Crossref.
7. Cherian BM, Leao AL, de Souza SF, Costa LMM, de Olyveira GM, Kottaisamy M, Nagarajan ER, Thomas S. Cellulose nanocomposites with nanofibres isolated from pineapple leaf fibers for medical applications. Carbohydrate Polymers, Elsevier, ScienceDirect. 2011 Oct 15; 86(4):1790–8. Crossref.
8. Kengkhetkit N, Amornsakchai T. Utilisation of pineapple leaf waste for plastic reinforcement: 1. A novel extraction method for short pineapple leaf fiber. Industrial Crops and Products, Elsevier, ScienceDirect. 2012 Nov; 40:55–61. Crossref.
9. El-Dib FI, Tawfik FM, Eshaq Gh, Hefni HHH, ElMetwally AE. Remediation of distilleries wastewater using chitosan immobilized bentonite and bentonite based organoclays. International Journal of Biological Macromolecules. 2016 May; 86:750–5. Crossref.
10. Mekkawi DME, Ibrahim FA, Selim MM. Removal of methylene blue from water using zeolites prepared from Egyptian kaolins collected from different sources. Journal of Environmental Chemical Engineering, Elsevier, ScienceDirect. 2016 Jun; 4(2):1417–22. Crossref.
11. Koshy N, Singh DN. Fly ash zeolites for water treatment applications. Journal of Environmental Chemical Engineering, Elsevier, ScienceDirect. 2016 Jun; 4(2):1460–72. Crossref.
12. Millar GJ, Couerthwaite SJ, Alyuz K. Behaviour of natural zeolites used for the treatment of simulated and actual coal seam gas water. Journal of Environmental Chemical Engineering, Elsevier, ScienceDirect. 2016 Jun; 4(2):1918–28. Crossref.
13. Olu-Owolabia BI, Alabi AH, Unuabonah EI, Diagboya PN, Bohm L, During RA. Calcined biomass-modified bentonite clay for removal of aqueous metal ions. Journal of Environmental Chemical Engineering. 2016 Mar; 4(1):1376–82. Crossref
14. Zarei-Baygi A, Moslemi M, Mirzaei SH. The combination of $KMnO_4$ oxidation and polymeric flocculation for the mitigation of membrane fouling in a membrane bioreactor. Separation and Purification Technology, Elsevier, ScienceDirect. 2016 Feb 8; 159:124–34. Crossref.
15. Zhang Y, Wang Y, Zhou L. Influence of excess $KMnO_4$ on the adsorption of powdered activated carbon. Chemical Engineering Journal, Elsevier, ScienceDirect. 2013 Jun 15; 226:279–85. Crossref.
16. Li J, Ren Y, Wang S, Ren Z, Yu J. Transition metal doped MnO2 nanosheets grown on internal surface of macroporous carbon for supercapacitors and oxygen reduction reaction electrocatalysts. Applied Materials Today, ScienceDirect. 2016 Jun; 3:63–72. Crossref.
17. Lin JL, Huang C, Pan, Ruhsing J, Wang YS. Fouling mitigation of a dead-end microfiltration by mixing-enhanced preoxidation for Fe and Mn removal from groundwater. Colloids and Surfaces A: Physicochemical and Engineering Aspects, Elsevier, ScienceDirect. 2013 Feb 20; 419:87–93. Crossref.
18. Wang M, Xu L, Zhai M, Peng J, Li J, Wei G. γ-ray radiation-induced synthesis and Fe(III) ion adsorption of carboxymethylated chitosan hydrogels. Carbohydrate Polymers, Elsevier, ScienceDirect. 2008 Nov 4; 74(3):498–503. Crossref.
19. Kousalya GN, Gandhi MR, Sundaram CS, Meenakshi S. Synthesis of nano-hydroxyapatite chitin/chitosan hybrid biocomposites for the removal of Fe(III). Carbohydrate Polymers, Elsevier, ScienceDirect. 2010 Oct 15; 82(3):594–9. Crossref.
20. Wu H, Yin Z, Quan Y, Fang Y, Yin C. Removal of methyl acrylate by ceramic-packed biotrickling filter and their response to bacterial community. Bioresource Technology, Elsevier, ScienceDirect. 2016 Jun; 209:237–45. Crossref.
21. Xie F, Liu G, Wub F, Guo G, Li G. Selective adsorption and separation of trace dissolved Fe(III) from natural water samples by double template imprinted sorbent with chelating diamines. Chemical Engineering Journal, Elsevier, ScienceDirect. 2012 Feb 15; 183:372–80. Crossref.
22. Sa DC, Benboudjema F, Thiery M, Sicard J. Analysis of microcracking induced by differential drying shrinkage. Cement and Concrete Composites, Elsevier, ScienceDirect. 2008 Nov; 30(10):947–56. Crossref.
23. Rasmussen ST, Okumu WN, Boenke K, O'Brien WJ. Optimum particle size distribution for reduced sintering shrinkage of dental porcelain. Dental Materials. 1997 Jan; 13(1):43–50. Crossref.
24. Uçer A, Uyanık A, Çay S, Ozkan Y. Immobilisation of tannic acid onto activated carbon to improve Fe(III) adsorption. Separation and Purification Technology, Elsevier, ScienceDirect. 2005 Jul; 44(1):11–7. Crossref.
25. Pastrana-Martinez LM, Lopez-Ramon MV, Fontecha-Camara MA, Moreno-Castilla C. Batch and column adsorption of herbicide fluroxypyr on different types of activated carbons from water with varied degrees of hardness and alkalinity. Water Research, Elsevier, ScienceDirect. 2010 Feb; 44(3):879–85. Crossref.
26. Shrestha S, Son G, Lee SH, Lee TG. Isotherm and thermodynamic studies of Zn(II) adsorption on lignite and coconut shell-based activated carbon fiber. Chemosphere, Elsevier, ScienceDirect. 2013 Aug; 92(8):1053–61. Crossref.
27. Mahmoud MA. Kinetics and thermodynamics of aluminum oxide nanopowder as adsorbent for Fe(III) from aqueous solution. Beni-Suef University Journal of Basic and Applied Sciences, Elsevier, ScienceDirect. 2015 Jun; 4(2):142–9. Crossref.
28. Gorrasi G, Milone C, Piperopoulos E, Lanza M, Sorrenti-

no A. Hybrid clay mineral-carbon nanotube-PLA nanocomposite films: preparation and photodegradation effect on their mechanical, thermal and electrical properties. Applied Clay Science, Elsevier, ScienceDirect. 2013 Jan; 71:49–54. Crossref.
29. Liu H, Yuan P, Qin Z, Liu D, Tan D, Zhu J, He H. Thermal degradation of organic matter in the interlayer clay–organic complex: A TG-FTIR study on a montmorillonite/12-aminolauric acid system. Applied Clay Science, Elsevier, ScienceDirect. 2013 Aug; 80–81:398–406. Crossref.
30. Msagati TAM, Mamba BB, Sivasankar V, Omine K. Surface restructuring of lignite by bio-char of cuminum cyminum –exploring the prospects in defluoridation followed by fuel applications. Applied Surface Science, Elsevier, ScienceDirect. 2014 May 15; 301:235–43. Crossref.
31. Athens GL, Shayib RM, Chmelka BF. Functionalization of mesostructured inorganic–organic and porous inorganic materials. Current Opinion in Colloid and Interface Science. 2009 Aug; 14(4):281–92. Crossref.
32. Berahman R, Raiati M, Mazidi MM, Paran SMR. Preparation and characterization of vulcanized silicone rubber/halloysite nanotube nanocomposites: effect of matrix hardness and HNT content. Materials and Design, Elsevier, ScienceDirect. 2016 Aug 15; 104:333–45. Crossref.
33. Mopoung S, Sriprang N, Namahoot J, Pumfang N, Chuayudom L, Rattanprasit W, Di-inkaew S, Jannachai K, Polkanyim D, Bunpum R. Functionalization and formation of drinking water filter rod from lignite with zeolite, bentonite, and clay. Carbon – Science and Technology. 2016; 8(1):55–62.
34. Yorgun S, Yıldız D. Preparation and characterization of activated carbons from Paulownia wood by chemical activation with H_3PO_4. Journal of the Taiwan Institute of Chemical Engineers, Elsevier, ScienceDirect. 2015 Aug; 53:122–31. Crossref.
35. Yahya MA, Al-Qodah Z, Ngah CWZ. Agricultural bio-waste materials as potential sustainable precursors used for activated carbon production: a review. Renewable and Sustainable Energy Reviews. 2015 Jun; 46:218–35. Crossref.
36. Mopoung S, Amornsakchai P, Somroop S. Characterization of phosphoric acid modified activated carbon fiber from fiber waste of pineapple leaf fiber production processing. Carbon – Science and Technology. 2016; 8(1):1–12.
37. Monier M, El-Sokkary AMA. Modification and characterization of cellulosic cotton fibers for efficient immobilization of urease. International Journal of Biological Macromolecules, Elsevier, ScienceDirect. 2012 Jul–Aug; 51(1–2):18–24. Crossref.
38. Yan Y, Cheng Q, Pavlinek V, Saha P, Li C. Fabrication of polyaniline/mesoporous carbon/MnO_2 ternary nanocomposites and their enhanced electrochemical performance for supercapacitors. Electrochimica Acta, Elsevier, ScienceDirect. 2012 Jun 1; 71:27–32. Crossref.
39. Wang Y, Wang X, Wang X, Liu M, Yang L, Wu Z, Xia S, Zhao J. Adsorption of Pb(II) in aqueous solutions by bamboo charcoal modified with $KMnO_4$ via microwave irradiation. Colloids and Surfaces A: Physicochemical and Engineering Aspects. 2012 Nov 20; 414:1–8. Crossref.
40. Luo C, Wei R, Guo D, Zhang S, Yan S. Adsorption behavior of MnO_2 functionalized multi-walled carbon nanotubes for the removal of cadmium from aqueous solutions. Chemical Engineering Journal, Elsevier, ScienceDirect. 2013 Jun 1; 225:406–15. Crossref.
41. San Cristóbal AG, Castelló R, Luengo MAM, Vizcayno C. Zeolites prepared from calcined and mechanically modified kaolins: a comparative study. Applied Clay Science, Elsevier, ScienceDirect. 2010 Jul; 49(3):239–46. Crossref.
42. Park EH, Jeong SU, Jung UH, Kim SH, Lee J, Nam SW, Lim TH, Park YJ, Yu YH. Recycling of sodium metaborate to borax. International Journal of Hydrogen Energy, Elsevier, ScienceDirect. 2007 Sep; 32(14):2982–7. Crossref.
43. He S, Chen W. Application of biomass-derived flexible carbon cloth coated with MnO_2 nanosheets in supercapacitors. Journal of Power Sources, Elsevier, ScienceDirect. 2015 Oct 30; 294:150–8. Crossref.
44. Wang M, Liu H, Huang ZH, Kang F. Activated carbon fibers loaded with MnO_2 for removing NO at room temperature. Chemical Engineering Journal, Elsevier, ScienceDirect. 2014 Nov 15; 256:101–6. Crossref.
45. Yaming L, Mingliang B, Zhipeng W, Run L, Keliang S, Wangsuo W. Organic modification of bentonite and its application for perrhenate (an analogue of pertechnetate) removal from aqueous solution. Journal of the Taiwan Institute of Chemical Engineers, Elsevier, ScienceDirect. 2016 May; 62:104–11. Crossref.
46. Slaty F, Khoury H, Wastiels J, Rahier H. Characterization of alkali activated kaolinitic clay. Applied Clay Science, Elsevier, ScienceDirect. 2013 May; 75–76:120–5. Crossref.
47. Xu J, Chen L, Qu H, Jiao Y, Xie J, Xing G. Preparation and characterization of activated carbon from reedy grass leaves by chemical activation with H_3PO_4. Applied Surface Science, Elsevier, ScienceDirect. 2014 Nov 30; 320:674–80. Crossref.
48. Foroushani FT, Tavanai H, Hosseini FA. An investigation on the effect of $KMnO_4$ on the pore characteristics of pistachio nut shell based activated carbon. Microporous and Mesoporous Materials. 2016 Aug; 230:39–48. Crossref.
49. van Garderen N, Clemens FJ, Mezzomo M, Bergmann CP, Graule T. Investigation of clay content and sintering temperature on attrition resistance of highly porous diatomite based material. Applied Clay Science, Elsevier, ScienceDirect. 2011 Apr; 52(1–2):115–21. Crossref.
50. Tunç T, Demirkıran AS. The effects of mechanical activation on the sintering and microstructural properties of cordierite produced from natural zeolite. Powder Technology, Elsevier, ScienceDirect. 2014 Jul; 260:7–14. Crossref.
51. Liu J, Gao X, Liu C, Guo L, Zhang S, Liu X, Li H, Liu C, Jin R. Adsorption properties and mechanism for Fe(III) with solvent impregnated resins containing HEHEHP. Hydro-

metallurgy, Elsevier, ScienceDirect. 2013 May; 137:140–7. Crossref.
52. Mopoung S, Bunterm T. $KMnO_4$ modified carbon prepared from waste of pineapple leaf fiber production processing for removal of ferric ion from aqueous solution. American Journal of Applied Sciences. 2016; 13(6):814–26. Crossref.
53. Sadeek SA, Negm NA, Hefni HHH, Wahab MMA. Metal adsorption by agricultural biosorbents: Adsorption isotherm, kinetic and biosorbents chemical structures. International Journal of Biological Macromolecules, Elsevier, ScienceDirect. 2015 Nov; 81:400–9. Crossref.
54. Xue Z, Li Z, Ma J, Bai X, Kang Y, Hao W, Li R. Effective removal of Mg^{2+} and Ca^{2+} ions by mesoporous LTA zeolite. Desalination, Elsevier, ScienceDirect. 2014 May 15; 341:10–8. Crossref.
55. Mopoung S, Bunterm T. Calcium ion removal by $KMnO_4$ modified pineapple leaf waste carbon prepared from waste of pineapple leaf fiber production processing. Carbon – Science and Technology. 2016 Jul 25; 8(4):13–9.